J Appl Electrochem (2014) 44:427–436
DOI 10.1007/s10800-014-0659-1

RESEARCH ARTICLE

Dependence of the electrocatalytic performance of platinized counter electrodes on the redox mediator employed in dye-sensitized solar cells

Seon Hee Seo · Sung Hwan Yoon · Mi Hyung Kim · Eun Ji Jeong · Hyon Chol Kang · Seung I. Cha · Dong Yoon Lee

Received: 16 September 2013 / Accepted: 2 January 2014 / Published online: 12 January 2014

Abstract The electrocatalytic properties of platinized counter electrodes (Pt CEs) prepared by various coating methods were investigated with respect to the redox mediator, including the widely used iodide/tri-iodide (I^-/I_3^-) and the more recently introduced cobalt(II/III)tris(2,2′-bipyridine) ($Co(bpy)_3^{2+/3+}$), for application in dye-sensitized solar cells (DSCs). The coating methods controlled Pt loading and the surface morphology of the Pt CEs. For a high-performance DSC with a fill factor >0.7, the charge-transfer resistance at the Pt CE/electrolyte interface should be <4.5 Ω cm^2 for both redox mediators. The I^-/I_3^--mediated DSCs were insensitive to Pt loading as low as 0.001 mg cm^{-2}, while the $Co(bpy)_3^{2+/3+}$-mediated DSCs required relatively large Pt loadings of > 0.005 mg cm^{-2}. Our results indicated that care should be taken in the preparation of Pt CEs with high transparency and low loading to obtain high-performance DSCs employing cobalt–ligand redox electrolyte.

Keywords Electrocatalyst · Counter electrode · Dye-sensitized solar cell

Electronic supplementary material The online version of this article (doi:10.1007/s10800-014-0659-1) contains supplementary material, which is available to authorized users.

S. H. Seo (✉) · S. H. Yoon · M. H. Kim · E. J. Jeong · S. I. Cha · D. Y. Lee
Nano Hydrid Technology Research Center, Korea Electrotechnology Research Institute, Changwon 641-120, Korea
e-mail: seosh@keri.re.kr

E. J. Jeong · H. C. Kang
Department of Advanced Materials Engineering, College of Engineering, Chosun University, Gwangju 501-759, Korea

1 Introduction

Dye-sensitized solar cells (DSCs) have been intensively studied as promising alternatives to solid-state solar cells due to their potential for low-cost solar energy conversion [1–3]. In contrast to other solar cells, a DSC is an electrochemical device with an electrolyte involving complex liquid junctions at a photoanode consisting of light-harvesting dyes adsorbed onto nanocrystalline wide-bandgap metal oxides, typically TiO_2 and a counter electrode (CE) of platinum nanoparticles (Pt NPs). Both electrodes are usually prepared on transparent conducting oxide (TCO) glass substrates, such as fluorine-doped tin oxide (FTO), and then assembled into a sandwich-type cell. The electrolyte contains a redox mediator, typically dissolved in an organic solvent, which efficiently regenerates the photo-oxidized dye and then shuttles the charge between the electrodes.

The iodide/tri-iodide (I^-/I_3^-) redox couple has been widely used as a redox mediator, but has some critical disadvantages [4–8] such as a highly corrosive nature and low electrochemical potential. To overcome these disadvantages, several alternatives to I^-/I_3^- have been suggested [9–13]. In particular, cobalt polypyridyl redox mediators have received considerable attention due to their high redox potential, reduced visible light absorption, and low corrosiveness [14, 15]. A high power conversion efficiency (PCE) of 12.3 % has been reported for a DSC with a cobalt(II/III)tris(2,2′-bipyridine) ($Co(bpy)_3^{2+/3+}$) redox electrolyte coupled with a specifically designed organic dye under simulated air mass 1.5 global (AM 1.5G) sunlight [16].

The CE catalyzes the electrochemical reduction of the oxidized form of the redox couple (I_3^- or $Co(bpy)_3^{3+}$) to the reduced form (I^- or $Co(bpy)_3^{2+}$) and must be able to fully support the charge required to generate photoelectrons at

the photoanode. Platinized conducting substrates have traditionally been used as a CE. The I^-/I_3^- redox reaction is a complex two-electron system ($I_3^- + 2e^- = 3I^-$) [17]. This type of complex reaction generally has slow charge-transfer kinetics, but dissociative chemisorption of iodine on the Pt surface substantially enhances the charge-transfer rate [7, 18]. In contrast to I^-/I_3^-, cobalt polypyridyl redox couples incorporate a simple one-electron outer-sphere reaction with low diffusivity. Cameron et al. [19] have pointed out that conventional Pt may not be ideal for the reduction of Co(II/III)-based redox couples due to its low exchange current density and then suggested the necessity of Pt nanostructuring. Alternatives that outperform Pt have been reported, such as porous conducting polymers [15, 20] and nanocarbons [21–23]. Control samples with Pt CEs had low fill factors (FF) of < 0.60 compared to those of alternative porous CEs for the reduction of the bulky Co-based redox mediators [24]. However, there have been few reports on optimal preparation and electrochemical properties of Pt CEs for high-performance Co(II/III)-mediated DSCs, in contrast to TiO_2 photoanodes combined with organic dyes [13–16, 25]. Pt electrodes remain worth considering because commercialization of DSCs is likely to begin with Pt CEs due to their higher transparency, low loading, and chemical/mechanical stability compared to other alternatives. Furthermore, fundamental electrochemical studies of platinized electrodes have generally involved Pt discs or sputter-deposited Pt films similar to bulk Pt [10, 14, 19, 26]. It may be informative to investigate heterogeneous charge-transfer behavior on platinized TCO electrodes with different loading and surface morphologies.

There are two main types of conventional Pt CEs: (1) Pt thin films with large crystallographic domains deposited by the sputtering method under high vacuum and (2) Pt NPs thermally prepared at $\sim$400 °C after drop-casting a diluted precursor solution or printing a viscous paste for large-scale fabrication. For cost-effectiveness, Pt loading should be minimized as much as possible. However, most reports of Co(II/III)-mediated DSCs have did described preparation conditions for Pt CEs in detail, and the minimum Pt loading has not been determined for high-performance Co(II/III)-mediated DSCs with a fill factor (FF) of > 0.7. In this study, recommended minimum Pt loading and maximum charge-transfer resistance at the Pt/electrolyte interface were determined for high-performance DSCs employing the widely used I^-/I_3^- and the recently introduced $Co(bpy)_3^{2+/3+}$ redox mediators. Platinized electrodes on FTO glass as a CE were prepared using three different coating methods for the application of DSCs: depositing thin films with a DC sputtering technique, screen-printing a viscous paste, and drop-casting a dilute precursor solution. The choice of coating methods determines Pt loading and the accessible surface area of the Pt CEs. The electrochemical performance of the Pt CEs was investigated using cyclic voltammetry, electrochemical impedance spectroscopy (EIS), and Tafel polarization curves to evaluate the reduction of two redox mediators. Pt loading and surface contamination of the Pt CEs affected the photovoltaic performances of DSCs employing I^-/I_3^- and $Co(bpy)_3^{2+/3+}$ redox electrolytes in combination with Ru-based N719 dye and carbazole MK-2 organic dye, respectively, each in optimized cell configurations in our laboratory.

2 Experimental details

2.1 Materials

Fluorine-doped tin oxides (FTO) glass (15 Ω sq^{-1}, Hartford) was used as conducting glass substrates. For iodide-mediated DSCs, the TiO_2 pastes were purchased from JGC Catalysts and Chemical Ltd. (PST-18NR for transparent layer and PST-400C for scattering layer). Commercial Pt pastes (Pt Catalyst T/SP), ruthenium polypyridyl dyes $Ru(II)LL'(NCS)_2$ (L = 2,2′-bipyridyl-4,4′-dicarboxylate, L' = 2,2′-bipyridyl-4,4′-ditetrabutylammonium carboxylate) (N719), and hot melt sealing foils were purchased from Solaronix. Hexylthiophene-functionalized carbazole dye named as MK-2 (2-cyano-3-[5‴-(9-ethyl-9*H*-carbazol-3-yl)-3′,3″,3‴,4-tetra-*n*-hexyl-[2,2′,5′,2″,5″,2‴]-quater thiophen-5-yl] acrylic acid) was purchased from Sigma-Aldrich. $Co(bpy)_3^{2+/3+}$-based redox mediators, $[Co(bpy)_3](PF_6)_2$ and its oxidized form $[Co(bpy)_3](PF_6)_3$, were synthesized according to references [14, 25]. Imidazolium salts are purchased from TCI and other chemicals obtained from Sigma-Aldrich.

2.2 Preparation of platinized counter electrodes

Platinized counter electrodes were prepared on FTO substrates using three different coating methods. One was a 0.5-μm-thick Pt thin film deposited by DC sputtering technique at room temperature, used as a CE without any further treatments. The others were prepared by screen-printing a commercial Pt paste and drop-casting 2 μL of $H_2PtCl_6{\cdot}6H_2O$ in 2-propanol with a micro-dispenser (Brand GMBH + CO KG: HandyStep® S) at room temperature. Pt loading of the drop-casted samples was adjusted by varying the concentration of the Pt precursor solution and/or by repeating the drop-cast deposition. After drying the solvent in air, the electrodes were fired at 400 °C for 30 min. All platinized electrodes were stocked in a vacuum oven at 45 °C before using.

2.3 Fabrication of dye-sensitized solar cells

Compact TiO_2 layers were firstly introduced on FTO substrates with diisopropoxytitanium bis(acetylacetonate) in 2-propanol followed by thermal treatment at 500 °C for 15 min. A mesoporous TiO_2 electrode was prepared on the compact layer and composed of a double-layer structure with a 14-μm-thick transparent layer and a 6-μm-thick scattering layer as explained elsewhere for the I^-/I_3^- redox mediator [27]. For the bulky $Co(bpy)_3^{2+/3+}$ redox mediator, 2.5-μm-thick transparent layer and a 6-μm-thick scattering layer were used as a photoanode. After annealing the photoanodes at 480 °C for 60 min, the sintered TiO_2 layers were immersed in 30 mM $TiCl_4$ aqueous solution for 30 min at 70 °C and then washed with deionized water. Finally, the $TiCl_4$-treated TiO_2 films were annealed at 450 °C for 30 min and then immersed in a 0.3 mM N719 ethanol solution for 21 h or 0.3 mM MK-2 toluene solution for 15 h at room temperature. The stained TiO_2 photoanode and the Pt CE were assembled with two sheets of Surlyn gaskets (SX1170-60) or a sheet (Meltonix 1170-25) to produce a sandwich-type cell for I^-/I_3^- or $Co(bpy)_3^{2+/3+}$ redox mediator, respectively. Iodide-mediated DSCs employed a liquid electrolyte consisting of 0.8 M 1,2-dimethyl-3-propylimidazolium iodide (DMPImI), 0.05 M LiI, 0.1 M I_2, 0.1 M guanidine thiocyanate (GuNCS), and 0.5 M 4-*tert*-butylpyridine (tBP) dissolved in acetonitrile. $Co(bpy)_3^{2+/3+}$-mediated DSCs incorporated an electrolyte consisting of 0.165 M $[Co(bpy)_3](PF_6)_2$, 0.045 M $[Co(bpy)_3](PF_6)_3$, 0.1 M $LiClO_4$, and 0.2 M tBP in acetonitrile.

For the best photovoltaic performances of DSCs in our laboratory, we used a thicker TiO_2 photoanode stained with N719 for the iodide-mediated DSCs with a gap of ~115 μm and a thinner photoanode stained with MK-2 for the $Co(bpy)_3^{2+/3+}$-mediated DSCs with a gap of ~23 μm. The electrolyte was injected into the cells through a hole on the CE by vacuum backfilling and sealed with a cover glass. For stable electrical contacts with cells to external circuit, the edges of FTO were ultrasonically soldered with metal wires (Cerasolzer alloy 186, MBR Electronics GmbH) for both photovoltaic and electrochemical measurements.

2.4 Measurements

Field-emission scanning electron microscopy (FE-SEM) was carried out on Hitachi S4800. Photocurrent density–voltage (*J*–*V*) characteristics were obtained using a Keithley model 2400 source measure unit. A 300 W Xenon lamp was used as a light source on Oriel solar simulator with air mass 1.5G filter, whose power of solar simulator was calibrated by a NREL-calibrated Si solar cell equipped with an IR-cutoff KG-5 filter. A black mask was applied on top of the cell, and then the photoactive area was defined to 0.196 cm^2.

Electrochemical characterizations were performed using a BioLogic SP-300 potentiostat. Cyclic voltammograms (CV) were measured in a three-electrode setup using an acetonitrile solution containing 10 mM 1,3-dimethylimidazolium iodide (DMImI), 2 mM I_2, and 0.1 M tetrabutylammonium hexafluorophosphate ($TBA{\cdot}PF_6$). For the measurements of $Co(bpy)_3^{2+/3+}$ redox mediator, an acetonitrile solution with 2 mM $Co(bpy)_3^{2+}$ and 0.1 M $TBA{\cdot}PF_6$ was used. A Pt plate and Ag/Ag^+ reference electrode (10 mM $AgNO_3$ and 0.1 M $TBA{\cdot}PF_6$ in acetonitrile) were used as counter and reference electrode, respectively. Studied electrodes were used as a working electrode in CV measurements. The scan rate was set at 100 mV s^{-1}.

Electrochemical impedance spectroscopy (EIS) and Tafel polarizations were performed using symmetrical closed dummy cells with two identical electrodes. The cells were assembled with 120- and 25-μm-thick Surlyn gaskets and filled with the iodide- and the $Co(bpy)_3^{2+/3+}$-based electrolyte used in DSCs, respectively. The impedance spectra were acquired under an open-circuit condition. The modulation amplitude was 10 mV in the frequency range of 0.1–100 kHz. EIS data were processed using ZSimpWin software.

3 Results and discussion

As described above, Pt CEs were prepared on conductive FTO glass substrates using three different coating methods to control Pt loading and the surface morphology. An image of the surface of a bare FTO is shown as a reference in Fig. 1a. The sputter-deposited Pt film (Pt sputter) followed the morphology of the bare FTO substrate (Fig. 1b). The Pt layer had a columnar structure with a thickness of 0.5 μm including many grain boundaries (Fig. 1c). The loading density of the Pt sputter was estimated at ~1 mg cm^{-2} based on the film thickness (Fig. 1c) and bulk volume density of Pt. The Pt sputter film was completely non-transparent to visible light (Fig. S1). Thermally prepared Pt electrodes had large agglomerates for screen-printed Pt (Pt paste), but homogeneously dispersed Pt NPs for drop-casted Pt with Pt precursor solutions (termed Pt 0.001 and Pt 0.005 based on the loading density, mg cm^{-2}) (Fig. 1d–f, respectively). The loading density of the Pt paste was calculated to be ~0.007 mg cm^{-2} by measuring the solid content of the Pt paste (~0.2 wt %) and the weight of the printed Pt paste on FTO substrate. When drop-casting a Pt precursor solution in alcohol, the conventionally used volume (10 μL cm^{-2} of 4.8 mM precursor solution) [13] induced inhomogeneous dispersion of the Pt NPs and metallic shiny gray color (Fig. S2). A volume

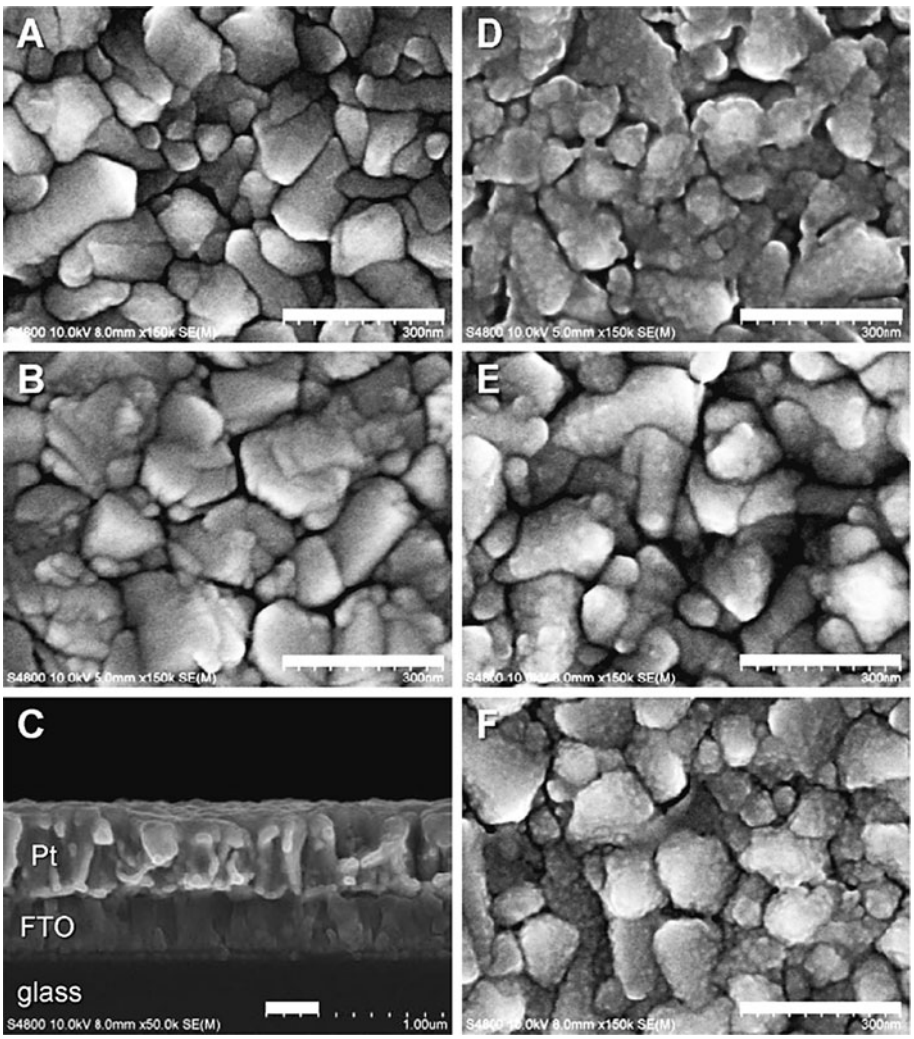

Fig. 1 SEM images of platinized counter electrodes on FTO glasses. **a** As-cleaned bare FTO, **b** Pt sputter, **c** cross-sectional Pt sputter, **d** Pt paste, **e** Pt 0.001, and **f** Pt 0.005. The *scale bar* corresponds to 300 nm

of about 7 μL cm^{-2} with low concentration of <2 mM was drop-casted, and a homogenous cauliflower-like morphology along the crystallographic domains of FTO was obtained for Pt 0.005 (Fig. 1f and Fig. S3). Pt 0.001 had low contrast to the bare FTO in the SEM images due to the very low Pt loading (Fig. 1e), but had a very weak and even gray color that could be visually distinguished from the bare FTO.

As finer features appear on the electrode surface, the active area is increased. To maximize the active area of the Pt NPs, Pt agglomerates should be avoided. The Pt paste sample with large agglomerates appeared to have a larger surface area than that of Pt 0.001; however, it was difficult to compare these surface areas with Pt 0.005 using SEM images. The effective surface areas of the Pt CEs could be compared on a relative basis using the effective double-layer capacitance obtained by fitting EIS data (see below). High accessible surface area is considered as a critical factor for electrocatalytic performance; therefore, these varying surface morphologies may result in differences in the electrochemical performance of the Pt CEs.

3.1 Cyclic voltammetry studies of the platinized electrodes

To investigate the electrocatalytic activities of the different platinized FTO electrodes for the reduction of the redox mediators, CVs were measured in a three-electrode configuration with dilute electrolytes incorporating I^-/I_3^- or $Co(bpy)_3^{2+/3+}$ redox mediators, at electrolyte compositions substantially different from those used in an optimized DSC. Figures 2a, b show the CVs of the platinized FTO electrodes in acetonitrile/0.1 M $TBA{\cdot}PF_6$ solutions containing DMImI (10 mM)/I_2 (2 mM) or $Co(bpy)_3^{2+}$ (2 mM), respectively, measured at a scan rate of 100 mV s^{-1}. The current density (J) divided by the geometric electrode areas was plotted rather than the current (I) because of the different electrode areas. In DSCs, an electrocatalytic material catalyzes the electrochemical reduction of the oxidized form of the redox mediator into the reduced form. Thus, the CV curves can be characterized using the cathodic peak current density ($J_{p,c}$) and the peak-to-peak separation potential (ΔE_{pp})

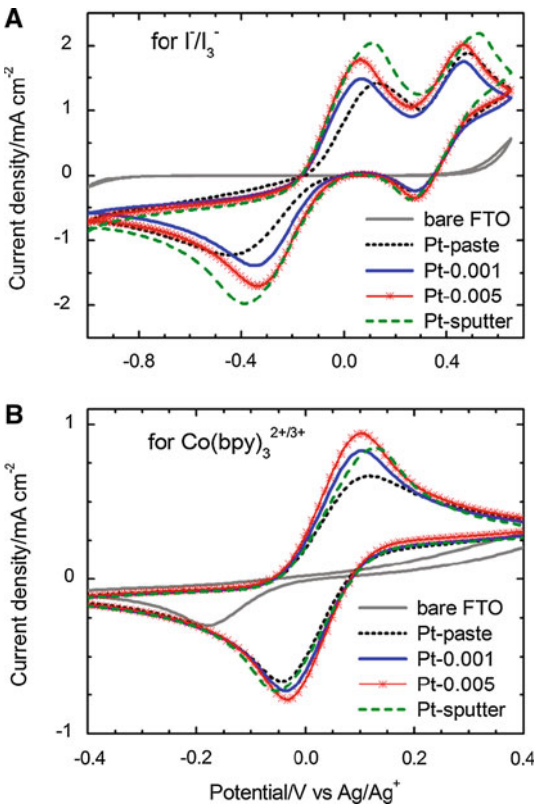

Fig. 2 Cyclic voltammograms of the different platinized FTO electrodes in acetonitrile/0.1 M TBA·PF_6 solutions containing **a** DMImI (10 mM)/I_2 (2 mM) or **b** $Co(bpy)_3^{2+}$ (2 mM), measured at 100 mV s^{-1}

[28]. In general, the $J_{p,c}$ depends on the concentration and diffusion coefficient of the electroactive species and the active surface area. Under a given measurement condition, the higher the $J_{p,c}$, the larger the electroactive surface area. A decrease in ΔE_{pp} corresponds to a higher rate of electron transfer at the electrode/electrolyte interface. Therefore, the electrocatalytic performance of CEs is determined by $J_{p,c}$ and ΔE_{pp}.

For the I^-/I_3^- redox couple, two pairs of redox reactions were observed on the Pt electrodes (Fig. 1a) as reported in previous studies [29, 30]. The cathodic peak at around −0.35 V corresponds to the reduction of I_3^- to I^-, and the peak at around +0.3 V corresponds to the reduction of I_2 to I_3^-. The electrocatalytic performance of the CEs is limited by the reduction of I_3^- as a minor carrier in I^-/I_3^--mediated DSCs and depends on the characteristics of the more negative pair of peaks. For the $Co(bpy)_3^{2+/3+}$ redox couple, the CVs demonstrated simple quasi-reversible behavior with an apparent ΔE_{pp} of 134 mV for Pt 0.005 (Fig. 2b). The $J_{p,c}$ of the $Co(bpy)_3^{2+/3+}$ redox reaction was substantially lower than that of I^-/I_3^-, mainly due to the low diffusion coefficient of the bulky $Co(bpy)_3^{2+/3+}$ redox couple; hence, Pt electrodes are believed to be an inappropriate catalyst for the reduction of Co–ligand complexes [19]. Interestingly, the bare FTO substrate had weak electrochemical activity for the reduction of $Co(bpy)_3^{3+}$ with a substantial negative shift of the cathodic peak potential and a low $J_{p,c}$ (Fig. 2b). However, such slow charge transfer did not work well as a CE for DSCs (Fig. S4). As a result, the effects of the bare FTO on the electrocatalytic performance of the platinized FTOs can be excluded.

The Pt sputter electrode without NPs had the highest $J_{p,c}$ for the I^-/I_3^- redox couple (Fig. 2a), contrary to expectations based on the SEM images (Fig. 1). This could be explained by the diffusion of the small I^-/I_3^- redox couple through the grain boundaries between columnar domains, increasing the active surface area. The Pt paste had inferior electrocatalytic performance for both redox couples based on the lower J_p and increased ΔE_{pp}. For the I^-/I_3^- redox couple, the ΔE_{pp} varied from 277.5 mV to 537.5 mV for Pt 0.005 and Pt paste, indicating that the charge-transfer rate for Pt paste was slower than for the other platinized electrodes. This may be because organic residues remained on the electrode surface after the thermal process, originated from a viscosity agent in the commercial Pt paste. Pt 0.001 had a similar ΔE_{pp} but inferior $J_{p,c}$ compared to Pt 0.005 for both redox couples, indicating that Pt 0.005 would be expected to have enhanced electrocatalytic performance due to its higher electroactive area. Based on the CV results, it appears that differences between the platinized electrodes mainly affected the reduction of I_3^- rather than $Co(bpy)_3^{3+}$.

3.2 Photovoltaic performance of DSCs

To examine the effect of the electrocatalytic activities estimated from the CV studies on photovoltaic performance, the platinized electrodes were applied in the DSCs as a CE for both types of redox mediators. The photovoltaic *J–V* curves are shown in Fig. 3, and the photovoltaic parameters are listed in Table 1. These results are optimized values for each system in our laboratory (I^-/I_3^- combined with N719 ruthenium-based dye and $Co(bpy)_3^{2+/3+}$ combined with MK-2 organic dye). The Pt loading and the surface morphology of the Pt CEs were not critical factors in the power conversion efficiency (PCE) of the I^-/I_3^--mediated DSCs, which ranged from 8.29 to 8.49 %. However, the effect of these factors was considerable on the PCEs of the $Co(bpy)_3^{2+/3+}$-mediated DSCs, which ranged from 5.11 to 6.31 % (Fig. 3). The electrocatalytic performance of the Pt CEs in the actual DSCs was somewhat contradictory to that of previous CV studies. This is likely due to differences in the concentrations of I_3^- and $Co(bpy)_3^{3+}$ used in the CV studies and for the DSCs. In the CV studies, dilute electrolytes were applied to exclude the effects of ion–ion repulsion interactions and of foreign adsorbed ions, and to focus on the charge-transfer kinetics

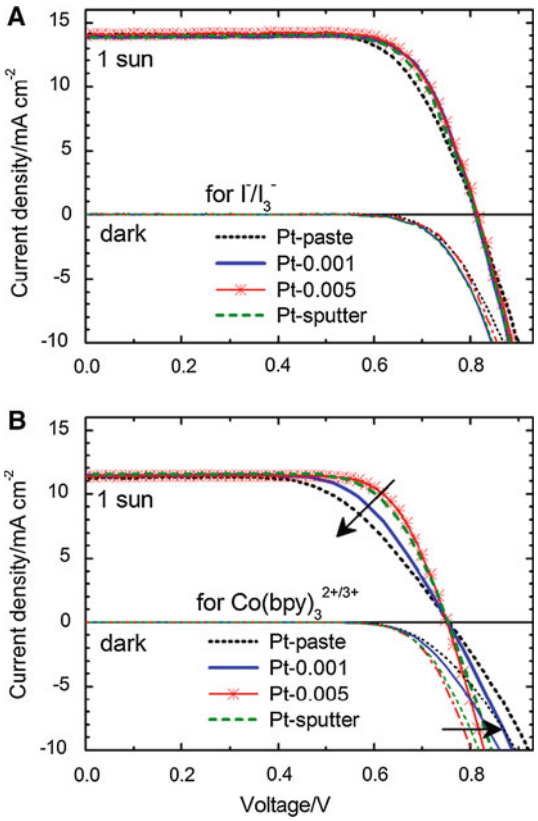

Fig. 3 Photovoltaic current density–voltage (J–V) curves of the DSCs employing different Pt CEs for **a** the I^-/I_3^-- and **b** the $Co(bpy)_3^{2+/3+}$-based electrolyte under the illumination of 100 mW cm^{-2} (1 sun) and in the dark

on the electrodes. Regarding the electrocatalytic performance of the CEs, a higher concentration of the electroactive species is preferred, but also has some undesirable effects in an actual device, such as an increase in the back reaction at the TiO_2 photoanode and a negative shift in the redox potential, leading to suppressed short-circuit current (J_{SC}) and open-circuit voltage (V_{OC}), eventually reducing the PCE of the DSCs [7]. Therefore, there is a limit to the ability to enhance the electrocatalytic performance of CEs by increasing the concentration of redox couples in the DSCs.

For the $Co(bpy)_3^{2+/3+}$-mediated DSCs, differences among the Pt CEs did not influence the V_{OC} ($\sim$0.754 V) or the J_{SC} ($\sim$11.38 mA cm^{-2}), but significantly suppressed the FF from 0.739 to 0.601. Therefore, the PCE was simply proportional to the FF, which directly associated with the electrocatalytic performance of the Pt CEs in our study. Interestingly, a substantial decrease in the dark current at a given bias voltage did not affect the V_{OC}, despite the conventional J–V relationship of $V_{OC} = (kT/q)\ln((J_{SC}/J_0) + 1)$ in solar cells [31, 32]. The dark current corresponds to the flow of charge from the TiO_2 photoanode to the CE through the electrolyte, which is induced by bias voltage in the opposite direction to the light current. Such suppressed dark current has been reported for DSCs, employing alternative CEs with low electrochemical performance for the reduction of the I^-/I_3^- redox couple [33, 34], and may result from decreased exchange current at the electrode/electrolyte interface [28]. Thus, a suppressed dark current with lower FF could be considered an indicator of low electrochemical performance of the CE used in the DSCs. The finely featured Pt CE of Pt 0.005 had high FF and PCE, the highest values for DSCs employing both $Co(bpy)_3^{2+/3+}$ redox electrolyte in combination with MK-2 dye reported to our knowledge [24, 35].

3.3 Charge-transfer resistance at the Pt CE/electrolyte interface

To investigate the charge-transfer processes at the Pt CE interface with electrolytes optimized for high-performance DSCs, EIS and Tafel polarization curves were measured

Table 1 Photovoltaic parameters of DSCs under the illumination of 100 mW cm^{-2} (1 sun) and EIS parameters of symmetrical closed dummy cells at an open-circuit voltage

Redox mediator	CE	V_{OC}/V	J_{SC}/mA cm^{-2}	FF	PCE/ %	R_0/Ω cm^2	R_{CT}/Ω cm^2	C_{eff}/μF cm^{-2}
[a]I^-/I_3^-	Pt paste	0.811	14.10	0.694	7.94	2.29	5.51	8.44
	Pt 0.001	0.811	13.89	0.746	8.41	2.29	2.67	7.87
	Pt 0.005	0.815	14.07	0.740	8.49	2.30	1.11	10.52
	Pt sputter	0.811	13.90	0.736	8.29	0.56	4.18	11.65
[b]$Co(bpy)_3^{2+/3+}$	Pt paste	0.756	11.24	0.601	5.11	2.06	9.25	10.23
	Pt 0.001	0.754	11.40	0.655	5.64	2.08	6.43	8.33
	Pt 0.005	0.751	11.37	0.739	6.31	2.05	1.52	12.26
	Pt sputter	0.754	11.50	0.704	6.11	0.13	4.49	12.46

[a] N719 dye and the iodide-based electrolyte (0.8 M DMPImI, 0.05 M LiI, 0.1 M I_2, 0.1 M GuNCS, 0.5 M tBP in acetonitrile) with two sheets of 60-μm-thick Surlyn as a spacer

[b] MK-2 dye and the $Co(bpy)_3^{2+/3+}$-based electrolyte (0.165 M $Co(bpy)_3{\cdot}(PF_6)_2$, 0.045 M $Co(bpy)_3{\cdot}(PF_6)_3$, 0.1 M $LiClO_4$, 0.2 M tBP in acetonitrile) with a sheet of 25-μm-thick Surlyn

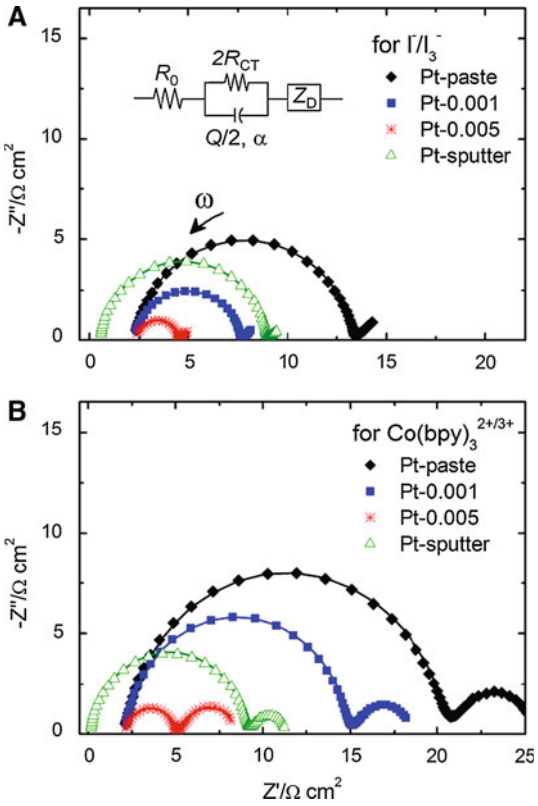

Fig. 4 Nyquist plots of the EIS data obtained under an open-circuit condition using symmetrical closed dummy cells for **a** the I^-/I_3^-- and **b** the $Co(bpy)_3^{2+/3+}$-based electrolyte. The *solid lines* are the fitted results based on the equivalent circuit in the *inset*

for symmetrical closed dummy cells consisting of two identical electrodes in the same configuration used in DSC [17]. Figure 4 shows EIS data measured under an open-circuit condition to avoid a mass-transfer limited region. The EIS exhibited typical reactive impedance (Z_{CT}) at the electrode/electrolyte interface in the high-frequency region, consisting of the charge-transfer resistance (R_{CT}) and the corresponding double-layer capacitance in parallel, and diffusion impedance (Z_D) of the redox mediators within the electrolyte in the low-frequency region (upon inspecting the Nyquist plot from left to right). The shape of the semi-infinite Warburg diffusion impedance Z_D depends on the ratio ($4D_O/d^2$) of the diffusion coefficient (D_O) of reactive species to the square of the spacer thickness (d) [36]. The shift of the impedances from the origin along the x-axis is associated with the frequency-independent ohmic resistance (R_0), and is related to the sheet resistance of the TCOs and the external electrical lead connection. The measured EIS data can be interpreted using an equivalent electrical circuit in the inset of Fig. 4a. For better fitting, a constant phase element (CPE) with an exponent α was adopted rather than capacitance, so that the apparent impedance can be expressed as

$$Z(\omega) = R_0 + \frac{2R_{CT}}{1 + (i\omega)^{\alpha} Q R_{CT}} + Z_D$$

where the parameters α and Q are independent of the frequency ω. The deviation of α from 1 represents the reactivity distribution of the electrode [37]. When $\alpha = 1$, the CPE behaves as a capacitor and R_{CT} is equal to the radius of a semicircle measured from the symmetrical dummy cells. The fitted results are plotted as solid lines in Fig. 4 and summarized for R_0, R_{CT}, and the effective double-layer capacitance (C_{eff}) in Table 1.

The Pt sputter sample covered the entire area of the FTO substrate, causing the sheet resistance of the conductive substrate to decrease due to the highly conductive metal layers. This in turn causes a low shift from the origin of the x-axis, with an R_0 of 0.56 Ω cm^2 compared to ~2.3 Ω cm^2 for the other Pt CEs in I^-/I_3^--based cells. The R_{CT} varied from 1.11 to 5.51 Ω cm^2 or 1.52 to 9.25 Ω cm^2 among the Pt CEs in the I^-/I_3^-- or the $Co(bpy)_3^{2+/3+}$-based electrolyte, respectively. Pt 0.005 had the lowest R_{CT}, but Pt paste had the highest, as expected based on the previous results. C_{eff} was also estimated from Q, α, and ω_{max} based on the following relationship as $C_{eff} = Q(\omega_{max})^{\alpha-1}$, where ω_{max} is the characteristic frequency at which the imaginary part of the impedance reaches its maximum [37]. The C_{eff} of Pt paste and Pt 0.001 was 8.44 and 7.87 μF cm^{-2} or 10.23 and 8.33 μF cm^{-2} in the I^-/I_3^-- and the $Co(bpy)_3^{2+/3+}$-based electrolytes, respectively (Table 1). Considering that double-layer capacitance is proportional to the accessible surface area of the electrode, the surface area of Pt paste must be larger than that of Pt 0.001. Despite that, the end product performance of the Pt paste CE was lower than that of Pt 0.001 in the DSCs, implying that the electrocatalytic performance of the CEs is not solely determined by the accessible surface area.

To emphasis the effect of R_{CT} on photovoltaic performance, the FF was plotted as a function of R_{CT} for both redox electrolytes (Fig. 5). Considering the highly electrocatalytic CEs should be able to support FFs higher than 0.7 in the DSCs, $R_{CT} < 4.5$ Ω cm^2 is required for both redox electrolytes. Thus, the I^-/I_3^--mediated DSCs were insensitive to the different Pt CEs, but the $Co(bpy)_3^{2+/3+}$-mediated DSCs were considerably affected by Pt loading and surface contamination of the Pt CEs. Conventional Pt pastes should be improved for application in Co(II/III)-mediated DSCs as an efficient CE.

3.4 Tafel polarization curves of the Pt CEs

To confirm the electrochemical characteristics of the Pt electrodes, Tafel polarization curves were measured for the symmetrical dummy cells used for EIS (Fig. 6). The

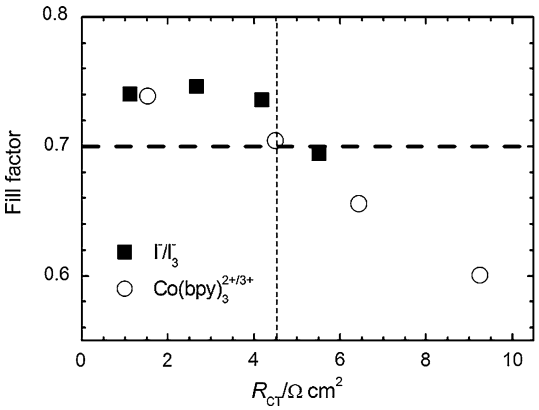

Fig. 5 Dependence of the fill factor on the charge-transfer resistance R_{CT} obtained by fitting the EIS data shown in Fig. 4

limiting current density (J_{lim}) depends on the diffusion of the redox couple in the thin-layer cell and can be approximated using Fick's first law as

$$J_{lim} = 2nFD_O\frac{C_O}{d}$$

where D_O is the diffusion coefficient of the reduced form of redox couples, d is the spacer thickness, C_O is the concentration, F is the Faraday constant, and n is the number of electrons involved in the electrode reaction [19]. From the J_{lim} obtained for Pt 0.005 under the given experimental conditions, the diffusion coefficients of I_3^- and $Co(bpy)_3^{3+}$ in acetonitrile solvent are 1.02×10^{-5} and 6.95×10^{-6} $cm^2\ s^{-1}$, respectively. These results are very close to the reported values of 1.1×10^{-5} and 6.4×10^{-6} $cm^2\ s^{-1}$, respectively [17, 21].

The rapid approach to a plateau, J_{lim}, having a steep slope indicates a high exchange current and then a somewhat higher electrocatalytic performance [29, 30]. These differences in the polarization curves are analogous to those of the photovoltaic J–V curves near open-circuit conditions ($J \rightarrow 0$) shown in Fig. 3. The FF can be affected by R_0, because there is an inverse relationship between the series resistance (R_{series}) and the FF. The R_{series}, defined as $R_0 + R_{CT} + R_D$, can be considered as a generalized approximation of the series resistance of DSCs, where R_D is the diffusion resistance of the electrolyte [36]. The Pt sputter had a substantially lower R_0 than the other Pt electrodes. Under given experimental conditions, the R_{series} is determined by the R_0 and R_{ct} of the symmetric cell. Based on Table 1, the R_{series} of Pt 0.001 (4.96 $\Omega\ cm^2$) was similar to that of Pt sputter (4.73 $\Omega\ cm^2$) for the I^-/I_3^- redox couple, which resulted in similar behavior (within experimental error) in the Tafel curves (Fig. 6a) and the J–V curves near open-circuit conditions (Fig. 4a).

The Tafel curves of Pt paste exhibited a considerably gentler slope and lower J_{lim}, indicating the lowest

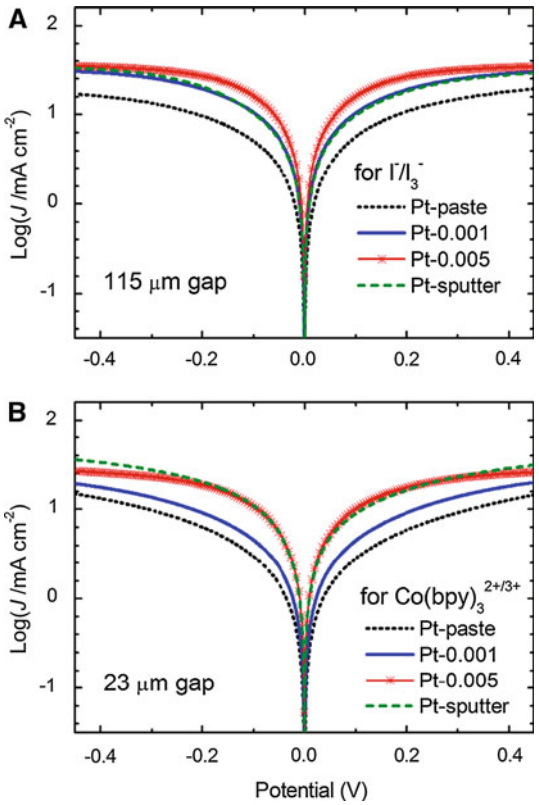

Fig. 6 Tafel polarization curves of the symmetrical dummy cells, the same used in EIS measurements in Fig. 4, with **a** the I^-/I_3^-- and **b** the $Co(bpy)_3^{2+/3+}$-based electrolytes

electrocatalytic performance among the Pt CEs for both redox electrolytes. The Pt 0.005 electrodes had the highest performance based on having the steepest Tafel slope. The Pt 0.001 had sufficient electrocatalytic performance in the I^-/I_3^- redox electrolyte, but not in the $Co(bpy)_3^{2+/3+}$. This suggests that a very small loading of 0.001 mg cm^{-2} is sufficient to achieve reasonable electrocatalytic performance of Pt CEs for I^-/I_3^--mediated DSCs. However, the bulky $Co(bpy)_3^{2+/3+}$ redox couple appears to require a higher Pt loading with a larger accessible surface area. To satisfy these requirements, the Pt loading should be >0.005 mg cm^{-2} with an R_{CT} of <4.5 $\Omega\ cm^2$ at the electrode/electrolyte interface for high-performance CEs in DSCs employing a bulky outer-sphere redox couple such as $Co(bpy)_3^{2+/3+}$.

4 Conclusions

The dependence of the electrocatalytic performances of various Pt CEs on two redox mediators, I^-/I_3^- and $Co(bpy)_3^{2+/3+}$, was investigated. We systematically examined the relationships between the photovoltaic and electrochemical properties of the Pt CEs with respect to the

redox couple. In this work, we determined the quantitative values of the minimum Pt loading [0.001 mg cm^{-2} for I^-/I_3^- and 0.005 mg cm^{-2} for $Co(bpy)_3^{2+/3+}$] and the upper limit of R_{CT} at the Pt CE/electrolyte interface ($\sim$4.5 Ω cm^2 for both redox couples) for high-performance DSCs with a FF larger than 0.7.

Acknowledgments This work was supported by a grant from Korea Electrotechnology Research Institute (KERI) and the "New & Renewable Energy Core Technology Program" of the Korea Institute of Energy Technology Evaluation and Planning (KETEP) granted financial resource from the Ministry of Trade, Industry & Energy, Republic of Korea (No. 2011T100100678).

References

1. Grätzel M (2001) Photoelectrochemical cells. Nature 414: 338–344
2. Pan K, Dong Y, Zhou W, Wang G, Pan Q, Yuan Y, Miao X (2013) TiO_2-B nanobelt/anatase TiO2 nanoparticle heterophase nanostructure fabricated by layer-by-layer assembly for high-efficiency dye-sensitized solar cells. Electrochim Acta 88:263–269
3. Miao X, Pan K, Liao Y, Zhou W, Pan Q, Tian G, Wang G (2013) Controlled synthesis of mesoporous anatase TiO_2 microspheres as a scattering layer to enhance the photoelectrical conversion efficiency. J Mater Chem A 1(34):9853–9861
4. Okada N, Matsui H, Kawashima T, Ezure T, Tanabe N (2004) 100 mm × 100 mm large-sized dye-sensitized solar cells. J Photochem Photobiol, A 164:193–198
5. Clifford JN, Palomares E, Nazeeruddin MK, Grätzel M, Durrant JR (2007) Dye dependent regeneration dynamics in dye sensitized nanocrystalline solar cells: evidence for the formation of a ruthenium bipyridyl cation/iodide intermediate. J Phys Chem C 111(17):6561–6567
6. Hamann TW, Farha OK, Hupp JT (2008) Outer-sphere redox couples as shuttles in dye-sensitized solar cells. Performance enhancement based on photoelectrode modification via atomic layer deposition. J Phys Chem C 112(49):19756–19764
7. Boschloo G, Hagfeldt A (2009) Characteristics of the iodide/triiodide redox mediator in dye-sensitized solar cells. Acc Chem Res 42(11):1819–1826
8. Hamann TW, Ondersma JW (2011) Dye-sensitized solar cell redox shuttles. Energy Environ Sci 4(2):370–381
9. Sapp S, Elliott M, Contado C, Caramori S, Bignozzi CA (2002) Substituted polypyridine complexes as efficient electron-transfer mediators in dye-sensitized solar cells. J Am Chem Soc 124(37):11215–11222
10. Wang M, Chamberland N, Breau L, Moser JE, Humphry-Baker R, Marsan B, Zakkeruddin SM, Grätzel M (2010) An organic redox electrolyte to rival triiodide/iodide in dye-sensitized solar cells. Nat Chem 2:385–389
11. Daeneke T, Kwon TH, Holmes AB, Duffy NW, Bach U, Spiccia L (2011) High-efficiency dye-sensitized solar cells with ferrocene-based electrolytes. Nat Chem 3:211–215
12. Zhou D, Yu Q, Cai N, Bai Y, Wang Y, Wang P (2011) Efficient organic dye-sensitized thin-film solar cells based on the tris(1,10-phenanthroline)cobalt(II/III) redox shuttle. Energy Environ Sci 4(6):2030–2034
13. Feldt SM, Kang W, Boschloo G, Hagfeldt A (2010) Effects of driving forces for recombination and regeneration on the photovoltaic performance of dye-sensitized solar cells using cobalt polypyridine redox couples. J Phys Chem C 115(43): 21500–21507
14. Feldt SM, Gibson EA, Gabrielsson E, Sun L, Boschloo G, Hagfeldt A (2010) Design of organic dyes and cobalt polypyridine redox mediators for high-efficiency dye-sensitized solar cells. J Am Chem Soc 132(46):16714–16724
15. Yum JH, Baranoff E, Kessler F, Moehl T, Ahmad S, Bessho T, Marchioro A, Ghadiri E, Moser JE, Yi C, Nazeeruddin MK, Grätzel M (2012) A cobalt complex redox shuttles for dye-sensitized solar cells with high open-circuit potentials. Nat Commun 3:631
16. Yella A, Lee H-W, Tsao HN, Yi C, Chandiran AK, Nazeeruddin MK, Diau EWG, Yeh CY, Zakeeruddin SM, Grätzel M (2011) Porphyrin-sensitized solar cells with Co(II/III)-based redox electrolyte exceed 12 percent efficiency. Science 334:629–634
17. Hauch A, Georg A (2001) Diffusion in the electrolyte and charge-transfer reaction at the platinum electrode in dye-sensitized solar cells. Electrochim Acta 46(22):3457–3466
18. Papageorgiou N (2004) Counter-electrode function in nanocrystalline photoelectrochemical cell configurations. Coord Chem Rev 248(13–14):1421–1446
19. Cameron PJ, Peter LM, Zakeeruddin SM, Gratzel M (2004) Electrochemical studies of the Co(III)/Co(II)$(dbbip)_2$ redox couple as a mediator for dye-sensitized nanocrystalline solar cells. Coord Chem Rev 248(13–14):1447–1453
20. Tsao HN, Burschka J, Yi C, Kessler F, Nazeerudding MK, Gratzel M (2011) Influence of the interfacial charge-transfer resistance at the counter electrode in dye-sensitized solar cells employing cobalt redox shuttles. Energy Environ Sci 4(12): 4921–4924
21. Kavan L, Yum JH, Grätzel M (2011) Graphene nanoplatelets outperforming platinum as the electrocatalyst in Co-bypyridine-mediated dye-sensitized solar cells. Nano Lett 11(12):5501–5506
22. Liao Y, Pan K, Wang L, Pan Q, Zhou W, Miao X, Jiang B, Tian C, Tian G, Wang G, Fu H (2013) Facile synthesis of high-crystallinity graphitic carbon/Fe_3C nanocomposites as counter electrodes for high-efficiency dye-sensitized solar cells. ACS Appl Mater Interfaces 5(9):3553–3670
23. Miao X, Pan K, Pan Q, Zhou W, Wang L, Liao Y, Tian G, Wang G (2013) High crystalline graphene/carbon black composite counter electrodes with controllable content: synthesis, characterization and application in dye-sensitized solar cells. Electrochim Acta 96:155–163
24. Stergiopoulos T, Falaras P (2012) Minimizing energy losses in dye-sensitized solar cells using coordination compounds as alternative redox mediators coupled with appropriate organic dyes. Adv Energy Mater 2(6):616–627
25. Kim HS, Ko SB, Jang IH, Park NG (2011) Improvement of mass transport of the $[Co(bpy)_3]^{II/III}$ redox couple by controlling nanostructure of TiO_2 films in dye-sensitized solar cells. Chem Commun 47(47):12637–12639
26. Liberatore M, Petrocco A, Caprioli F, Mesa CL, Decker F, Bignozzi CA (2010) Mass transport and charge transfer rates for Co-(III)/Co-(II) redox couple in a thin-layer cell. Electrochim Acta 55(12):4025–4029
27. Seo SH, Kim SY, Koo BG, Cha SI, Lee DY (2010) Influence of electrolyte composition on the photovoltaic performance and stability of dye-sensitized solar cells with multiwalled carbon nanotube catalysts. Langmuir 26(12):10341–10346
28. Bard A, Faulkner LR (2001) Potential sweep methods. Electrochemical methods fundamentals and applications, kinetics of electrode reactions, 2nd edn. Wiley, New Jersey, pp 228–236
29. Imoto K, Takahashi K, Yamaguchi T, Komura T, Nakamura J, Murata K (2003) High-performance carbon counter electrode for dye-sensitized solar cells. Sol Energy Mater Sol Cells 79(1): 459–469

30. Wang Y, Wu M, Lin X, Shi Z, Hagfeldt A, Ma T (2012) Several highly efficient catalyst for Pt-free and FTO-free counter electrodes of dye-sensitized solar cells. J Mater Chem 22(9): 4009–4014
31. Sze SM (1981) Solar cells. Physics of semiconductor devices, 2nd edn. Wiley, New York, p 794
32. Ito S, Liska P, Comte P, Charvet R, Péchy P, Bach U, Schmidt-Mende L, Zakeeruddin SM, Kay A, Nazeeruddin MK, Grätzel M (2005) Control of dark current in photoelectrochemical (TiO_2/I^-–I_3^-) and dye-sensitized solar cells. Chem Commun 41(34): 4351–4353
33. Ramasamy E, Lee WJ, Lee DY, Song JS (2008) Spray coated multi-wall carbon nanotube counter electrode for tri-iodide (I_3^-) reduction in dye-sensitized solar cells. Electrochem Commun 10(7):1087–1089
34. Kavan L, Yum JH, Grätzel M (2011) Optically transparent cathode for dye-sensitized solar cells based on grapheme nanoplatelets. ACS Nano 5(1):165–172
35. Murakami TN, Koumura N, Uchiyama T, Uemura Y, Obuchi K, Masaki N, Kimura M, Mori S (2013) Recombination inhibitive structure of organic dyes for cobalt complex redox electrolytes in dye-sensitised solar cells. J Mater Chem A 1(3):792–798
36. Fabregat-Santiago F, Bisquert J, Garcia-Belmonte G, Boschloo G, Hagfeldt A (2005) Influence of electrolyte in transport and recombination in dye-sensitized solar cells studied by impedance spectroscopy. Sol Energy Mater Sol Cells 87:117–131
37. Orazem ME, Tribollet B (2008) Electrochemical impedance spectroscopy, chapter 13. Wiley, New Jersey